


# Multichannel Wearable fNIRS-EEG System for Long-Term Clinical Monitoring

Ali Kassab <sup>1,\*</sup> Jérôme Le Lan,<sup>2</sup> Julie Tremblay,<sup>3</sup> Phetsamone Vannasing,<sup>3</sup> Mahya Dehbozorgi,<sup>2</sup> Philippe Pouliot,<sup>2,5</sup> Anne Gallagher,<sup>3</sup> Frédéric Lesage,<sup>2</sup> Mohamad Sawan,<sup>2</sup> and Dang Khoa Nguyen<sup>1,4</sup>

<sup>1</sup>Research Center, Centre Hospitalier Universitaire de Montréal, Université de Montréal, Montréal, Québec H2X 0A9, Canada

<sup>2</sup>Department of Electrical Engineering, École Polytechnique de Montréal, Montréal, Québec H3T 1J4, Canada

<sup>3</sup>Research Center, Hôpital Sainte-Justine, Université de Montréal, Montréal, Québec H3T 1C4, Canada

<sup>4</sup>Department of Neurology, Hôpital Notre-Dame (Centre Hospitalier de l'Université de Montréal), Montréal, Québec H2L 4M1, Canada

<sup>5</sup>Research Center, Montreal Heart Institute, Montréal, Québec H1T 1C8, Canada



**Abstract:** Continuous brain imaging techniques can be beneficial for the monitoring of neurological pathologies (such as epilepsy or stroke) and neuroimaging protocols involving movement. Among existing ones, functional near-infrared spectroscopy (fNIRS) and electroencephalography (EEG) have the advantage of being noninvasive, nonobstructive, inexpensive, yield portable solutions, and offer complementary monitoring of electrical and local hemodynamic activities. This article presents a novel system with 128 fNIRS channels and 32 EEG channels with the potential to cover a larger fraction of the adult superficial cortex than earlier works, is integrated with 32 EEG channels, is light and battery-powered to improve portability, and can transmit data wirelessly to an interface for real-time display of electrical and hemodynamic activities. A novel fNIRS-EEG stretchable cap, two analog channels for auxiliary data (e.g., electrocardiogram), eight digital triggers for event-related protocols and an internal accelerometer for movement artifacts removal contribute to improve data acquisition quality. The system can run continuously for 24 h. Following instrumentation validation and reliability on a solid phantom, performance was evaluated on (1) 12 healthy participants during either a visual (checkerboard) task at rest or while pedalling on a stationary bicycle or a cognitive (language) task and (2) 4 patients admitted either to the epilepsy ( $n = 3$ ) or stroke ( $n = 1$ ) units. Data analysis confirmed expected hemodynamic variations during validation recordings and useful clinical information during in-hospital testing. To the best of our knowledge, this is the first demonstration of a wearable wireless

Additional Supporting Information may be found in the online version of this article.

Contract grant sponsor: Canadian Institutes of Health Research (CIHR); Contract grant number: MOP 133643; Contract grant sponsor: Heart and Stroke Foundation of Canada in Partnership with CIHR; Contract grant numbers: 01001-000, 01006-000; Contract grant sponsor: National Sciences and Engineering Research Council in partnership with CIHR; Contract grant number: CPG-127774.

\*Correspondence to: Ali Kassab; Hôpital Notre-Dame du CHUM, 1560 Sherbrooke East, Montréal, Québec H2L 4M1, Canada. E-mail: ali.kassab@umontreal.ca

Received for publication 23 June 2017; Revised 2 October 2017; Accepted 8 October 2017.

DOI: 10.1002/hbm.23849

Published online 23 October 2017 in Wiley Online Library (wileyonlinelibrary.com).

multichannel fNIRS-EEG monitoring system in patients with neurological conditions. *Hum Brain Mapp* 39:7–23, 2018. © 2017 Wiley Periodicals, Inc.

**Key words:** portable near-infrared spectroscopy; electroencephalography; cerebral hemodynamics; functional brain imaging and monitoring; limb-shaking transient ischemic attacks; epilepsy

## INTRODUCTION

Functional neuroimaging techniques such as positron emission tomography (PET), single-photon emission computed tomography (SPECT) and functional magnetic resonance imaging (fMRI) have allowed significant advances in our understanding of the brain and its disorders. Each has its methodological strengths and limitations. Limitations include their bulkiness, high cost, exposure to radiation (PET, SPECT), high sensitivity to movement, complex statistical analysis (fMRI), need for the participant to lie down in a confined area, and inability for continuous monitoring. Functional near-infrared spectroscopy (fNIRS) is an emerging noninvasive, nonionizing, and relatively low-cost neuroimaging technique that uses the ability of light in the near-infrared spectrum (700–1,000 nm) to penetrate biological tissue to assess changes in oxyhemoglobin (HbO<sub>2</sub>), deoxyhemoglobin (Hb), blood volume, and tissue oxygen availability with high temporal resolution [Jöbsis et al., 1977; Ferrari et al., 1985; Villringer and Chance, 1994]. Technical and methodological advances have allowed fNIRS to become a relevant research tool in neuroscience [Wolf et al., 2007; Leff et al., 2011; Ferrari and Quaresima, 2012; Torricelli et al. 2014; Ehlis et al., 2014; Boas et al., 2014; Kopton and Kenning, 2014; Naseer and Hong, 2015; Mihara and Miyai, 2016] and as a clinical tool in the evaluation and monitoring of critically ill neonates and infants notably during cardiac surgeries [Edmonds et al., 2004; Denault et al., 2007; Murkin and Arango, 2009; Cerbo et al. 2012].

Briefly, near-infrared light is projected onto the scalp by optical fibers (sources) and transmitted through the skull [Lloyd-Fox et al., 2010; Scholkmann et al., 2014]. Photons penetrate and propagate diffusely into superficial brain tissue. While some photons are absorbed by chromophores (mainly hemoglobin), others are reflected back and captured by sensor probes (detectors) placed at a certain distance from transmitting optical fibers. By using one wavelength more sensitive to Hb (e.g. 735 nm) and another more sensitive to HbO<sub>2</sub> (e.g. 830 nm), variations in amplitude of backscattered light can be used to infer on local changes in blood oxygenation [Delpy et al., 1988; Cooper et al., 1996]. Furthermore, assuming a constant hematocrit, changes in total hemoglobin (HbT = HbO<sub>2</sub> + Hb) can be used as a proxy of cerebral blood volume (CBV) variations [Madsen and Secher, 1999]. In essence, fNIRS is a neuroimaging technique based on the same fundamental principles underlying the pulse

oximeter. However, while the latter is a tool now widely used in hospitals to monitor peripheral blood oxygenation, brain fNIRS has had only timid penetration in clinical research and practice [Obrig, 2014]. This is partly explained by the following limitations of current fNIRS systems: a) many have a small number of channels limiting spatial sampling; b) some restrict optodes to the forehead to avoid hair contamination due to the low acquisition chain sensitivity; c) the majority are neither truly compact (wearable), nor wireless, hampering its use at the bedside or in fields requiring mobility (e.g. rehabilitation); d) all do not seamlessly integrate simultaneous electroencephalography (EEG) monitoring (the only other technique that can monitor brain activity for long duration at the bedside) when required.

To answer the growing need for a portable device allowing to monitor electrical and hemodynamic brain activities in clinical settings, we sought to develop a wearable and wireless high channel count fNIRS-EEG system to record changes in HbO<sub>2</sub>, Hb, HbT and EEG on a portable personal computer. The current paper presents a safe and robust high-channel-count combined fNIRS-EEG prototype composed of 32 infrared light sources, 32 photodetectors, and up to 32 EEG channels. Each source can be coupled to four detectors, offering a total of 128 fNIRS channels. In addition to standard measurements on a tissue-equivalent phantom, we present the validation and performance of our prototype through a series of mobile and stationary tasks on healthy subjects as well as preliminary experience with the prototype in diverse clinical settings.

## MATERIALS AND METHODS

### General Description of the Portable fNIRS-EEG Prototype and Headgear

Our system is composed of a full head cap with optodes and a control module, linked together with light electrical wires. Three lightweight (~ 200 g) NIRS-EEG caps were designed to accommodate different head sizes to allow the sensor elements to maintain an orthogonal orientation to the scalp: small (head circumference < 53 cm), medium (53–58 cm) and large (> 58 cm). These full-head caps were made of elastic bands and integrated 3D-printed round plastic sockets designed to maintain probes and electrodes in place in close contact with the skin. Sockets were separated from each other by a small gap ranging from 2.5 to 3.5 cm, thereby allowing us to have an average source-

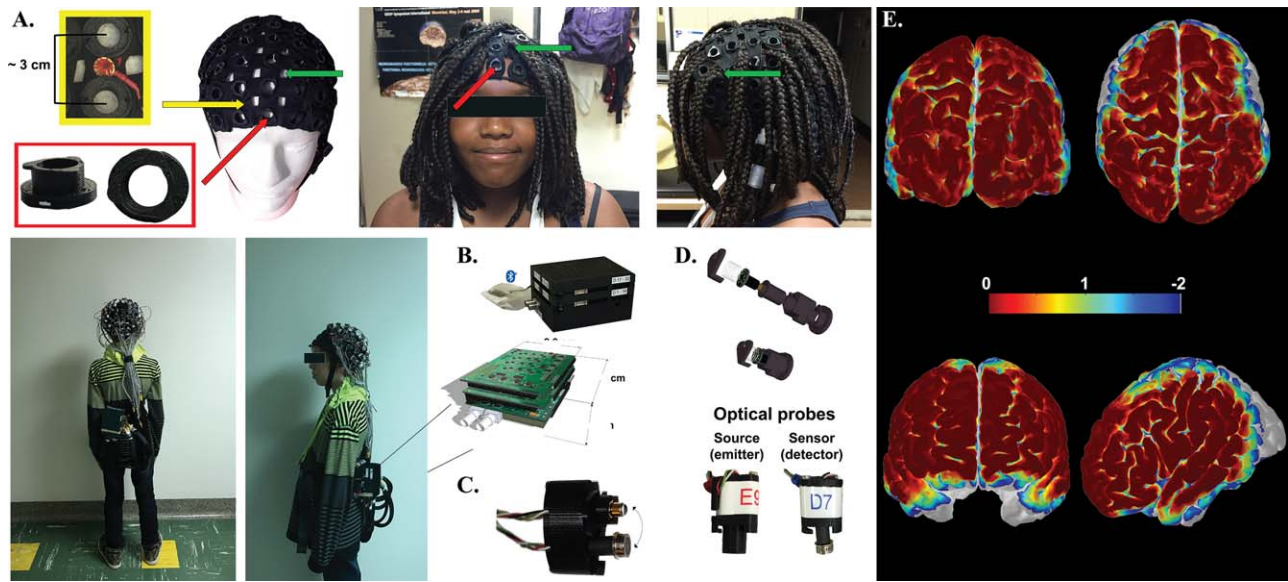


**Figure 1.**

NIRS-EEG prototype parts including fNIRS-EEG caps (A), control module (B), double optodes to gather signal from superficial layers (C), and optode design (D). Spatial sensitivity profile generated with AtlasViewer [Aasted et al. 2015] for each measurement channel for the visual (top) and language (bottom) task (E). Yellow arrow shows the integration of EEG electrodes between NIRS sockets (red arrows). Opening (wholes) in the cap (green arrows) allow better removal of dense long hair.

detector distance of  $\sim 3$  cm. A hole within sockets allowed users free access to move hair aside from the light path before fastening the optodes. A dark woolen fabric worn over the optical probes served to improve probe-tissue-contact and shield ambient light. A questionnaire was used to assess subject comfort during installation and recording.

NIRS emitter and detector circuits fit on  $0.95 \text{ cm}^2$  round printed-circuit boards (PCB) that are packaged in a 3D-printed plastic housing to plug into cap connectors. Inside the housing, a smooth spring pushes the sensor towards the head, providing improved light coupling between scalp and optode, limiting infrared light scattering between the cap and the scalp, while connector design prevents ambient light pollution. Furthermore, we developed a separate connector and socket that can combine both emitter and detector for short distance (1 cm) channels. This optode is meant to measure extracortical hemodynamics.

The prototype can retrieve information from the 128 fNIRS channels and 32 EEG channels (Fig. 1). During an acquisition, the control module gathers 8 EEG and 4 NIRS data samples at a time, then proceeds with data packing and sends them on a serial port towards a computer through a universal serial bus (USB) cable or a Bluetooth bridge device. A graphical user interface (GUI) developed with LabVIEW retrieves data packets for real-time processing. The GUI can display a total of 294 curves (256 NIRS

curves for 128 channels times 2 wavelengths, 32 EEG curves, one curve for the digital triggers, 3 accelerometer curves and 2 auxiliary analog curves) and record them for post-processing. The power consumption during an acquisition using 32 emitters and 32 detectors at full illumination is 2.4 W when a USB cable is used, and 2.6 W with the Bluetooth link. In the worst-case scenario, with the 7.4 V, 10 Ah batteries, the prototype can run an acquisition uninterrupted over a period of 24 hours (Fig. 2).

### EEG and NIRS Circuitry

The EEG acquisition chain consists of amplification and filtering of the difference between measurement and reference electrodes. An instrumentation amplifier at the front-end cuts the common mode interference and noise while amplifying the signal by 100, then a bandpass filter is applied between 0.1 and 100 Hz, and the signal is once again amplified by 100. A reference circuit places the head at a potential of 2.5 V which contains feedback signals from two electrodes placed on the left and right mastoids for common mode interference rejection. The EEG acquisition chain is separated as much as possible from the NIRS chain for crosstalk elimination and parallelism implementation. Located in the control module, the four 8-channel analog-to-digital converter (ADCs) dedicated to EEG signals digitize data in parallel with the NIRS signals through their own serial peripheral interface (SPI) bus, recording

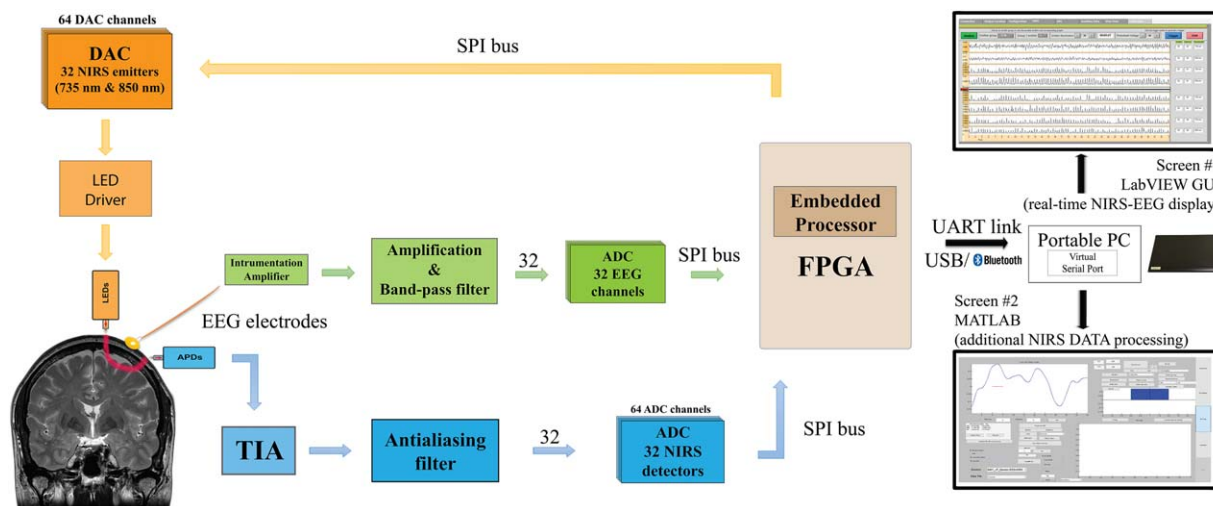


**Figure 2.**  
Global architecture of NIRS-EEG prototype.

320 samples per second for each channel with a resolution of 16 bits.

The NIRS emitter is a small size two-wavelength (735 & 850 nm) light-emitting diode (LED) from Epitex, and the detector is an avalanche photodiode (APD) S2384 from Hamamatsu coupled with a transimpedance amplifier (TIA) circuit, embedded on the round PCB; the current-voltage gain is set at 10 MV/A, with a measured 3 dB frequency cut-off of 28 kHz. A negative high voltage (around -150V), generated on the control module by a high-voltage direct current (DC)-to-DC converter regulator (EMCO, CA02-5N), biases all the APDs to provide enough sensitivity to detect diffused infrared light and is current-limited for patient protection.

On the control module, eight 8-channel digital-to-analog converters (DAC) set the illumination intensity for both wavelengths of each emitter, while four 8-channel ADCs, preceded by anti-aliasing filters, digitized amplified TIA measurements with a resolution of 16 bits. As the light sources are not modulated, but only time-multiplexed to decrease power consumption and increase safety, the duration of light emission and detection has to be as short as possible to allow sampling from all 128 channels in 1/20<sup>th</sup> of a second (20 Hz). This was made possible by maximizing the frequency cut-off value of the TIA. For each wavelength of every emitter, a stabilizing period of time precedes the sampling of the four coupled detectors. For each detector, 8 samples are averaged, and 8 other samples taken in the dark are subtracted to reject ambient lighting and interchannel crosstalk, improving SNR.

LED power consumption is drastically decreased by time-multiplexing: the pulse duration is equal to 390  $\mu$ s. At maximal LED illumination, the equivalent total illumination power is 140  $\mu$ W for each wavelength, reducing the risks of tissue heating. The duty cycle of the gathered

emitters is 0.5, meaning that the light emission is equivalent to one LED emitting 50% of the time. Sensitivity was, furthermore, improved by maximizing the gain of APDs: the bias voltage is set separately for each APD through potential dividers adapting the unique high voltage signal coming from the regulator.

### Digital Architecture

The embedded circuitry consists of three stacked PCBs and battery for a total size of  $12 \times 9 \times 7$  cm<sup>3</sup> and a weight of 650 g. The first PCB contains an Altera Cyclone III low-power Field-Programmable Gate Array, flash memory and random-access memory to control through SPI buses the acquisition chains of different modules. It also contains the high-voltage regulator and its controlling circuitry, several regulators for different voltage supplies (5 V for analog parts and 3.3 V for digital parts), and the protection and low-power-detection circuits for a rechargeable Li-Ion 7.4 V, 10 Ah battery. An accelerometer is included on this same PCB, providing movement information along the three axes at a rate of 50 Hz for each axe. Two additional external 3D accelerometers can be added on the subject's head if necessary. This data can be used to quantify movement during a task (e.g. gait), and help distinguish, after an acquisition, artifact movement from hemodynamic variations. Also, two Bayonet Neill-Concelman (BNC) connectors can be used to plug an external analog signal for simultaneous digitalization at 340 Hz with 12-bit resolution, for example, electrocardiogram or analog trigger. An optical isolation on SPI lines prevents the prototype from being possibly connected to the power grid, protecting the patient from leakage path. Eight digital triggers complete the additional features; these help identify and synchronize with data 256 different events during event-related

potential protocols. The two other PCBs are identical and contain the 32 EEG acquisition chains (16 on each board), and the DACs and ADCs for infrared light illumination and detection, the anti-aliasing filters, and the connectors towards the sensors and electrodes.

The link between the control module and the computer is either a UART RS-232 serial port emulated on a USB cable by a FTDI chip, or a Bluetooth serial port module (OBS421 from connectBlue), able to transmit the required 328 kbps bit rate during an acquisition. The developed communication protocol includes transfer error detection and allows ulterior interpolation of data if packets are lost during their transmission. Through USB cable, the number of lost data is negligible, contrary to Bluetooth communication, where interferences and set-up modifications can alter signal quality; in this case, the protocol can support signal loss for three seconds without the need to start over an acquisition. The data is sent to a LabVIEW-based interface which provides a user-friendly GUI for interaction with the hardware allowing easy configuration of important system parameters and data acquisition. Prior to an acquisition, the user is invited to configure specific parameters: for each emitter, its illumination power, and its four associated detectors, and the APD common bias voltage. These parameters and comments are recorded in a configuration file along with data, and can be imported from a previous acquisition. A calibration window helps detect if one curve is saturating or does not receive enough light, indicating a need to change a parameter or verify optode installation. In addition to manual calibration, the software has an auto-calibration function that can increase or reduce the emitted light in order to obtain adequate SNR. The curves are recorded in real-time in a LabVIEW format. A Matlab script imports data towards HomER format [Huppert et al., 2009] for further in depth data processing.

### Phantom Studies

For phantom validation studies, we used a solid optical phantom made of polyester resin, to which India ink was added as an attenuation agent and  $\text{TiO}_2$  as a diffusive agent (coefficient at a wavelength of  $\lambda = 758 \text{ nm} = 0.017 \text{ mm}^{-1}$  and diffusion coefficient  $= 0.7 \text{ mm}^{-1}$ ). After coupling one single detector to one single light source at 4 cm of distance, we first applied different light intensities and avalanche gains to study the influence of these factors on baseline value and noise amplitude to DC level ratio. Then a 1 Hz sinusoidal light signal similar to in vivo signals was injected in the phantom to compute the SNR with different avalanche gains.

### Patient Population

We then conducted signal validation experiments on 12 healthy (6 males, age: 13–27 years) adults and children using either a visual task or two standard language

paradigms. The prototype was subsequently tested in four distinct clinical scenarios on patients: a) a patient with limb-shaking transient ischemic attacks admitted to the stroke unit; b) a patient admitted at the epilepsy monitoring unit (EMU); c) a patient admitted to the intensive care unit for status epilepticus; d) a patient undergoing language lateralization assessment in the neuropsychology department. Experiments were approved by our ethics committee and informed consent was obtained from all participants.

### Validation and Performance Studies

Preferential coverage allowing higher spatial sampling of certain areas of interest was privileged for these experiments: bilateral occipito-parieto-precentral regions for visual experiments (Fig. 3A) and bilateral fronto-temporo-parietal regions for language experiments (Fig. 4A). To ensure that the same brain areas were measured in each subject, optodes localization was determined in relation to the 10–20 system. We further measured the distance from three fiducial points (nasion, left and right pre-auricular) to the horizontal level at Fp1/Fp2, T3 and T4 respectively, and took front and side pictures before and after to verify if any shifting had occurred. To account for installation time and constant probe installation across participants, all installations were done by the same individuals (AK, PV). Visual and language stimuli were presented electronically using E-Prime 2.0 software (Psychology Software Tools, Pittsburgh, PA) and a BNC digital output cable was used to send trigger signals directly to our prototype.

To evaluate the mobility of our system, a modified version of the experiment performed in Piper et al. (2014) was done during the first validation protocol (Fig. 3A). It consisted of a visual pattern reversal task (subject B1 to B8) while participants were sitting on a training bicycle that was installed in an acoustically shielded and dimmed room. The task was performed twice: 1) a first time while the participants were sitting still on the bicycle and 2) a second time while the participants were pedalling at an average pace of 15 km/h (10–20 km/h). To evaluate the quality of our EEG (and ERPs), we used stackable jumper/linker cables to simultaneous recording electrophysiological signals with a commercial EEG system (Neuroscan SynAmps2 EEG/EP, Compumedics Ltd.). The signals were amplified by Neuroscan Synamp amplifiers (Compumedics, Charlotte, NC, USA), digitized at a rate of 500 Hz and recorded by Neuroscan Scan 4 Acquire Software (Compumedics, Charlotte, NC, USA).

The second validation protocol consisted of a language study (Fig. 4A). The handedness of all participants was assessed using the Edinburgh Inventory [Oldfield, 1971]. Four French-speaking participants (subjects L1 to L4) underwent one session of fNIRS recording. The language experimentation included expressive (verbal fluency) and receptive (passive story listening) language tasks in a

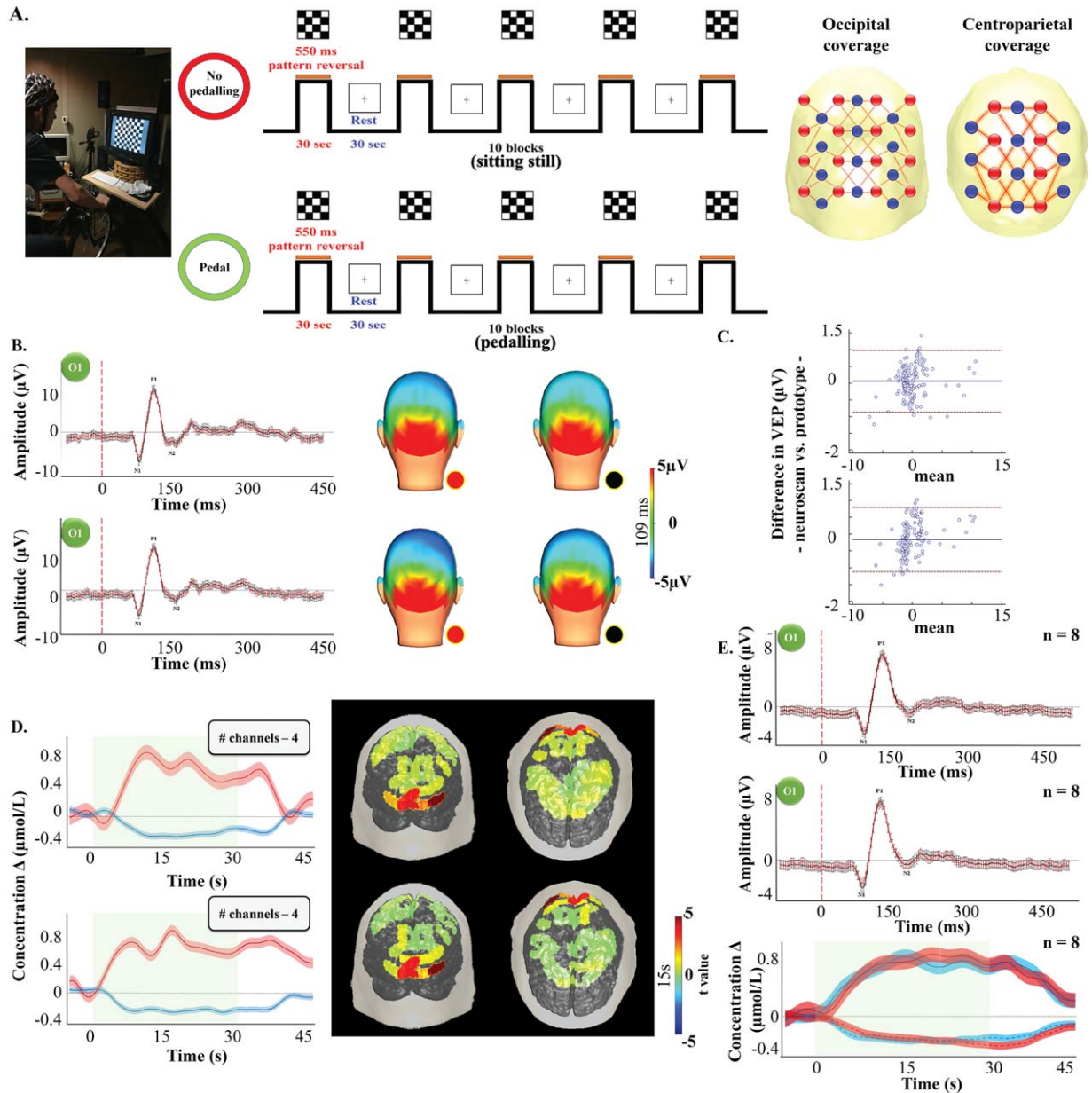


**Figure 3.**

Channel layout and description of the visual paradigm (A). P100 time course and topography over the visual cortex averaged along every stimulation blocks while sitting still (upper row) and pedalling (bottom row) for participant B4. Black line/dot: Neuroscan system. Red line/dot: fNIRS-EEG prototype (B). Results from the Bland–Altman analysis for the P<sub>100</sub> amplitude changes at rest (left) and while pedalling (right) between our prototype and Neuroscan. Dotted red line: limits of agreement. Solid blue line: bias (C).  $\Delta[\text{HbO}_2]$  (red line)/ $\Delta[\text{Hb}]$  (blue line) time courses over the visual cortex and  $\Delta[\text{HbO}_2]$  topography (15 s), with

color-coded t value after Bonferroni-correction for multiple comparison ( $P < 0.0004$ ), averaged over 8 visual stimulation periods in subject B4 obtained from 5 channels over the visual cortex while sitting still (upper row) and pedalling (bottom row). Red and blue shaded area: standard error of the mean for  $\Delta[\text{HbO}_2]$  and  $\Delta[\text{Hb}]$ , respectively. Green shaded area: stimulation period (D). Average P100 time course from all 8 participants obtained with our system (solid red line) and the Neuroscan system (solid black line) while sitting still (first row) and pedalling (second row) (E).

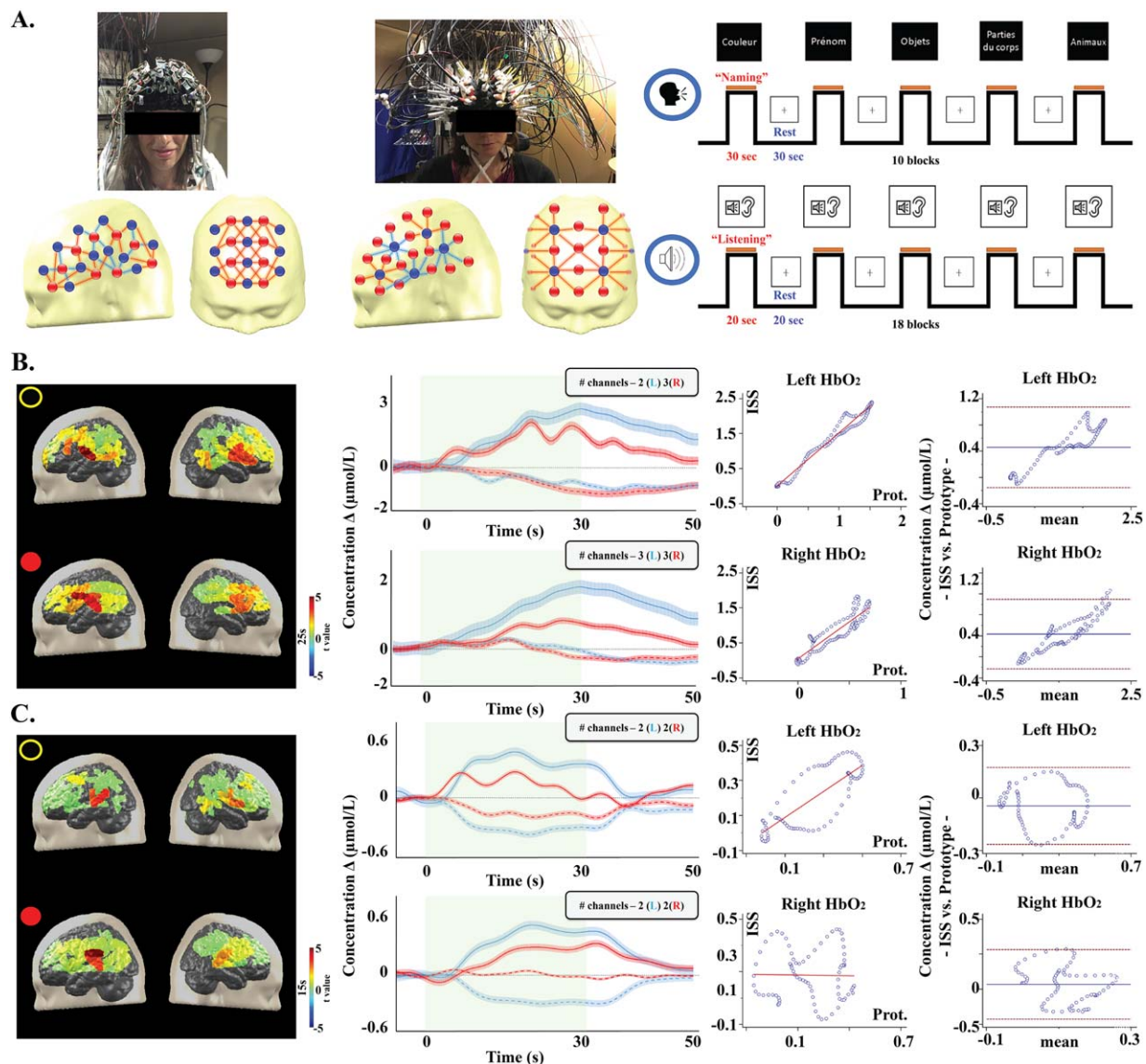


Figure 4.

Channel layout and description of the language paradigm (A).  $\Delta[\text{HbO}_2]$  topography (15 s), with color-coded  $t$  value after Bonferroni correction, and  $\Delta[\text{HbO}_2]$  (straight line)/ $\Delta[\text{Hb}]$  (dotted line) time courses over the Broca area along all stimulation blocks during the listening task in subject L3 and results from the linear regression and Bland-Altman analysis for  $\Delta[\text{HbO}_2]$  (B).  $\Delta [\text{HbO}_2]$  topography (15 s), with color-coded  $t$  value after

Bonferroni correction, and  $\Delta[\text{HbO}_2]$  (straight line)/ $\Delta[\text{Hb}]$  (dotted line) traces over the Wernicke area averaged along all stimulation blocks during the naming task in the same subject and results from the linear regression and Bland-Altman analysis for  $\Delta[\text{HbO}_2]$  (C). Black dot/first row: ISS system. Red dot/second row: fNIRS-EEG prototype. Left side: blue line. Right side: red line. Dotted red line: limits of agreement. Solid blue line: bias.

block design paradigm [Gallagher et al. 2007]. To evaluate the quality of the fNIRS component, we performed for each participant a second recording within 4–6 weeks using a well-established multi-channel frequency-domain device spectrometer (Imagent Tissue Oxymeter, ISS Inc., Champlain, Illinois, USA) composed of 50 laser diodes (690 nm and 830 nm) modulated at 110.0 MHz and 16

photomultiplier tube detectors. Optical intensity (DC), modulation amplitude (AC), and phase data were acquired in a block design paradigm with a sampling rate of 15 Hz by its own software (ISS Corporations “Boxy”). DC and AC data were filtered using a band-pass filter of 0.1–0.001 Hz, normalized by dividing each value by the mean value across time points for each block and channel,

and transformed to quantify concentration changes of HbO<sub>2</sub> and Hb for each channel. Channels were selected based on the standard error of phase variations across trials.

An anatomically specific montage was created based on a normalized structural template from the Montreal Neurological Institute or the patient's own MRI to ensure that optical fibres were placed over the region(s) of interest (ROI). This was done using a stereotaxic system (Brain-sight TM Frameless39, Rogue Research, Canada), which enables the transfer of ROI, determined by MRI, onto the cap. This procedure allowed us to obtain the best possible montage in terms of source-detector number and locations of the targeted regions for each participant.

## Data Processing and Signal Analysis

### Processing of the EEG signal

Offline analysis of the raw EEG data was done using with Brain Vision Analyzer 2.0 (Brain Products GmbH, Munich). The pre-processing of the EEG data obtained from the visual task was done in five steps. First, we referenced electrodes to both linked mastoids and down-sampled to 256 Hz. Second, the data was filtered (1–50 Hz) to remove high- and low-frequency waves and was visually inspected to check for artifacts. Third, we performed an independent component analysis to correct for eye movement artifacts, before segmenting at –100 ms before the stimulus onset and ending at 500 ms after the stimulus onset. In a next step, we used the semiautomatic artifact rejection tool to exclude segments having a minimum and maximum amplitude difference of more than 100  $\mu$ V. Finally, visually evoked potentials (VEPs) were obtained by averaging time series from –200 to 500 ms of pattern reversal presentations. As for the clinical EEG, a careful examination for interictal spikes and seizures was performed by an expert electroencephalographer (DKN).

### Comparison of EEG signals between systems

To quantitatively assess the EEG data obtained from our prototype, an unpaired t-test ( $p < 0.05$ ) was performed against the EEG data acquired by the commercial EEG system (i.e. Neuroscan SynAmps2) after averaging all VEPs obtained while a) sitting still or b) pedalling. Furthermore, to visualize the agreement between the VEPs (fNIRS-EEG prototype vs. Neuroscan), we used the Bland-Altman method with 95% limits of agreement ( $SD \pm 1.96$ ) [Bland and Altman, 1986, 1996].

### Processing of the fNIRS signal

All NIRS data were first processed with the toolbox HomER [Huppert et al., 2009]. First, every channel was bandpass-filtered between 0.05 and 0.1 Hz to retrieve the slow hemodynamic variations while eliminating slower

drifts. Channels with a raw DC intensity at the level of the equipment noise or with a standard deviation higher than 20% were considered as artefactual and excluded from the analysis. Second, the relative changes in HbO<sub>2</sub> and Hb for each measurement position were calculated from the raw light intensity by applying the modified Beer-Lambert law [Kocsis et al., 2006]. For each healthy participant, concentration changes in HbO<sub>2</sub> and Hb were averaged across the blocks. A differential pathlength factor (DPF = 5.9 at 830 nm and DPF = 6.5 at 735 nm) and partial pathlength factor (PPF = 0.50 at 830 nm and 0.50 at 735 nm) correction was also applied to generate concentration values [Duncan et al. 1995; Kohri et al. 2002]. All concentrations represent a variation during activation relative to baseline values, thus are expressed as delta concentrations. Third, significant activation (i.e. delta concentration amplitude > baseline noise) in the regions of interest (ROIs) for visual (i.e. visual cortex) and language (i.e. Broca's area, Wernicke's areas, and contralateral homologous regions) tasks, as well as for clinical monitoring (e.g. epileptic focus) were identified by computing a two-tailed paired t-test and were further used to qualitatively assess the results. Finally, to account for multiple comparisons, p-values were Bonferroni-corrected, setting the significance level after correction to  $p = 0.05$ . The t-values of the significant  $\Delta$ HbO<sub>2</sub> channels were color-coded and partially projected onto the gray matter surface of the MNI standard brain model or own MRI scan.

### Comparison of fNIRS signals between systems

For the visual task, we used an unpaired (student's) t-test ( $p < 0.05$ ) to test for differences in the mean value of HbO<sub>2</sub> and Hb between 10 s and 30 s after activation onset between the two conditions (i.e. sitting vs. pedalling) during visual stimulation. Group averages for each condition were also calculated. Time course of  $\Delta$ HbO<sub>2</sub> and  $\Delta$ Hb are displayed with their standard error of mean (SEM). The Dice similarity coefficient (DSC) was used to compare visual mapping obtained with each condition [Dice LR, 1945]. Based on the literature [Zijdenbos et al., 1994; Fleiss JL, 1982] a  $DSC \geq 0.80$  was deemed to reflect very good concordance between maps, a  $DSC \geq 0.70$  was deemed to reflect good concordance between maps, and a  $DSC < 0.70$  was associated with poor concordance. Finally, a one-way ANOVA on DSC values was performed to compare fNIRS visual mapping concordance between the two conditions. For the language tasks, we performed an unpaired (student's) t-test ( $p < 0.05$ ) to compare mean values of HbO<sub>2</sub> and Hb (10 s to 30 s and 5 s to 20 s after activation onset for the fluency and listening task respectively) between our prototype and ISS. Group averages for each language task and for each system were also calculated. We also calculated a language lateralization index (LI) in the left (LH) and right (RH) hemisphere ROIs [Pujol et al., 1999; Seghier, 2008]:  $(LH - RH)/(LH + RH)$ , where L is the maximal increase in HbO<sub>2</sub> associated with the naming or semantic



**TABLE I. Average electrophysiological and hemodynamic changes during the visual task**

Participant (sex, age, profession)	Screen distance (cm)	Hair description	Installation time (min)	Comfort scale	VEP <sup>Prot.</sup> ( $\mu$ V)		VEP <sup>Neuroscan</sup> ( $\mu$ V)		$\Delta$ HbO <sub>2</sub> $\Delta$ Hb ( $\mu$ mol)		# Reje- cted trials		Dice (HbO <sub>2</sub> )
					S	P	S	P	S	P	S	P	
					<b>B1 (F, 21, student)</b>	155	Straight, redheaded, medium	48	9	4.31	4.83	4.53	
<b>B2 (M, 24, engineer)</b>	138	Straight, black, short	40	6	3.27	5.48	3.74	6.35	0.64	1.12	1	2	1.00
<b>B3 (M, 28, engineer)</b>	142	Curly, black, short	51	8	4.63	5.99	5.16	6.24	0.32	0.31	2	2	1.00
<b>B4 (F, 22, student)</b>	155	Dreads, black, long	77	10	9.89	9.89	10.54	10.39	0.86	0.84	1	0	0.82
<b>B5 (M, 17, student)</b>	153	Straight, blond, medium	53	9	8.06	8.3	7.51	9.03	0.65	0.82	0	0	0.72
<b>B6 (M, 13, student)</b>	150	Straight, black, medium	61	7	5.92	5.58	5.86	5.4	1.04	1.21	2	2	0.90
<b>B7 (M, 15, student)</b>	150	Straight, black, short	47	8	4.59	4.53	4.99	4.55	0.77	0.86	2	3	0.82
<b>B8 (F, 26, student)</b>	134	Curly, black, long	63	9	6.03	6.63	5.91	6.46	0.73	1.06	0	1	0.82

M: male; F: female; VEP: visually evoked potential; HbO<sub>2</sub>: oxy-hemoglobin; Hb: deoxy-hemoglobin; Prot.: prototype; Neuroscan: commercial EEG system; S: sitting still; P: pedaling.

language task, obtained from an averaged curve of all channels covering left Broca’s and Wernicke’s areas and R is the HbO<sub>2</sub> value obtained from an average curve of all channels covering the right mirror regions of left Broca’s and Wernicke’s areas measured at the same time as the maximal left increase in HbO<sub>2</sub>. A value  $< -0.10$  indicates right hemisphere language dominance, a value  $> 0.10$  indicates left hemisphere language lateralization and a value close to zero ( $-0.10 \leq LI \leq 0.10$ ) reveals a bilateral language distribution. Concordance between individual language lateralization (or LI) results was computed from both systems using unweighted kappa statistics, which consists of comparing the results of HbO<sub>2</sub> LIs from our prototype and HbO<sub>2</sub> LIs from ISS. Quantitative comparison of hemodynamic changes between our system and ISS was done using the same Blant-Altman method previously described. Under the assumption of independence of measurements, we took every 25<sup>th</sup> measurement of  $\Delta$ HbO<sub>2</sub> and  $\Delta$ Hb [Chandrasekaran B. 1971; Cox and Wermuth, 1996]. Qualitative comparison of maps of language activations between the two systems was performed qualitatively.

## RESULTS

### Phantom Validation

We first carried out some long acquisitions on polyester resin phantom mimicking tissue to confirm software and prototype capability to maintain signal quality over time.

Beyond slow drifts associated with LED heating that can be filtered out in post-processing, the system was able to record low level signal without significant change in SNR over time. Over 24 continuous hours, the software was able to record every curve with no data loss. The standard deviation of the signal on phantom (calculated on periods of 60 seconds) was constant and equal to 1.2 mV (for a 5 V ADC input range) from the beginning to the end of the recording.

### Physiological Validation

Table I shows the demographic characteristics, recording information, comfort scores and results for each participant. Five adults (2M) and three children (3M) were recorded using simultaneously our prototype and the commercial EEG system. As expected, the checkerboard protocol showed a clear and significant ( $p < 0.05$ ) VEP and fNIRS activations over the visual areas in all participants during both conditions (i.e. sitting still and pedalling). No significant electrophysiological (VEP) or hemodynamical (fNIRS) responses were seen over the precentral and parietal regions.

During the non-pedalling condition, our system recorded a mean  $P_{100}$  peak amplitude of  $5.80 \pm 0.44 \mu$ V (time = 109 ms) while a peak amplitude of  $5.96 \pm 0.43 \mu$ V (time = 109 ms) was recorded with Neuroscan. During the pedalling condition, mean  $P_{100}$  peak amplitudes of  $6.49 \pm 0.48 \mu$ V (time = 109 ms) and  $6.74 \pm 0.49 \mu$ V (time = 109 ms) were recorded with our system and the Neuroscan, respectively.

Individual and group comparison showed no statistical differences for both  $P_{100}$  peak amplitudes and latencies measured by the two systems. Linear regression comparing our device to the commercial one showed a group average correlation coefficient of  $r = 0.99$  ( $p < 0.0001$ ) during the non-pedalling condition and  $r = 0.99$  ( $p < 0.0001$ ) during the pedalling condition. Bland-Altman plot showed a group average difference of  $-0.01 \mu\text{A}$  (limits of agreement were  $-0.34$  to  $0.31 \mu\text{A}$ ) during the non-pedalling condition and  $-0.02 \mu\text{A}$  (limits of agreement were  $-0.38$  to  $0.33 \mu\text{A}$ ) during the pedalling conditions (Fig. 3B–E). On an individual basis, statistical comparison of the time course between the two conditions (i.e. sitting vs. pedalling) while performing the visual-task showed, for both systems, a statistically significant difference in three participants (B01, B02, B08) (Supporting Information, Fig. 1).

Both sitting still and pedalling generated a positive  $\text{HbO}_2$  and negative Hb response over visual areas (V1 and V2) during visual stimulation. In the absence of pedalling, we observed a mean peak hemodynamic response average across all participants of  $0.71 \pm 0.08 \mu\text{mol/L}$  for  $\text{HbO}_2$  and  $-0.34 \pm 0.04 \mu\text{mol/L}$  for Hb. During pedalling, a mean  $\text{HbO}_2$  increase of  $0.69 \pm 0.08 \mu\text{mol/L}$  and a Hb decrease of  $-0.28 \pm 0.04 \mu\text{mol/L}$  was observed. For the channels reaching a significant level of activation, individual-level analysis between the two conditions showed a significant difference for the mean  $\Delta\text{HbO}_2$  time courses in all participants, while the mean Hb time courses showed a significant difference in 50% of participants. Activation maps comparison between the two conditions showed very good concordance ( $\text{DSC} \geq 0.80$ ) for cortical visual mapping in seven out of eight (88%) participants (mean  $\text{DSC} = 0.89 \pm 0.04$ ). The one-way ANOVA results showed no statistical differences between groups for  $\text{DSC}$  ( $p = 0.074$ ).

For language tasks, all participants were right-handed and spoke French as their first language. Participant demographics, setup time and comfort scale are presented in Table II. During the passive listening task, our prototype recorded over posterior temporal regions a significant  $[\text{HbO}_2]$  increase ( $p = 0.03$ ) and  $[\text{Hb}]$  decrease ( $p = 0.01$ ), larger on the left (Wernicke) ( $x \Delta[\text{HbO}_2]_{\text{L}} = 0.85 \pm 0.07 \mu\text{mol/L}$ ,  $x \Delta[\text{Hb}]_{\text{L}} = -0.45 \pm 0.04 \mu\text{mol/L}$ ) than the right ( $\Delta[\text{HbO}_2]_{\text{R}} = 0.41 \pm 0.04 \mu\text{mol/L}$ ,  $\Delta[\text{Hb}]_{\text{R}} = -0.25 \pm 0.03 \mu\text{mol/L}$ ) in three participants (L1, L3, L4). Subject L2 exhibited a larger  $[\text{HbO}_2]$  increase ( $\Delta[\text{HbO}_2]_{\text{L}} = 0.10 \pm 0.02 \mu\text{mol/L}$  vs.  $\Delta[\text{HbO}_2]_{\text{R}} = 0.72 \pm 0.02 \mu\text{mol/L}$ ) and  $[\text{Hb}]$  decrease ( $[\text{Hb}]_{\text{L}} = -0.18 \pm 0.06$  vs.  $\Delta[\text{Hb}]_{\text{R}} = -0.45 \pm 0.04$ ) over the right posterior temporal region. In comparison, the ISS also recorded a significantly larger  $[\text{HbO}_2]$  increase ( $x \Delta[\text{HbO}_2]_{\text{L}} = 0.84 \pm 0.07 \mu\text{mol/L}$  vs.  $x \Delta[\text{HbO}_2]_{\text{R}} = 0.51 \pm 0.03 \mu\text{mol/L}$ ) ( $p = 0.04$ ) and  $[\text{Hb}]$  decrease ( $x \Delta[\text{Hb}]_{\text{L}} = -0.34 \pm 0.04 \mu\text{mol/L}$  vs.  $x \Delta[\text{Hb}]_{\text{R}} = -0.25 \pm 0.03 \mu\text{mol/L}$ ) ( $p = 0.04$ ) over the left posterior temporal area in L1, L3, L4 and a larger  $[\text{HbO}_2]$  increase ( $\Delta[\text{HbO}_2]_{\text{L}} = 0.85 \pm 0.06 \mu\text{mol/L}$  vs.  $\Delta[\text{HbO}_2]_{\text{R}} = 1.72 \pm 0.02 \mu\text{mol/L}$ ) and  $[\text{Hb}]$  decrease ( $[\text{Hb}]_{\text{L}} = -0.21 \pm 0.04$  vs.  $\Delta[\text{Hb}]_{\text{R}} = -0.69 \pm 0.06$ )

over the right posterior temporal area in L2. For both systems, laterality index (LI) computed from the maximum  $[\text{HbO}_2]$  peak over Wernicke's area and the contralateral homologous region showed left hemisphere dominance for receptive language in participant L1, L3 and L4 and right dominance for participant L2 ( $\kappa = 1.0$ ,  $p < 0.0001$ ). Mean time to peak for  $\text{HbO}_2$  was  $16 \pm 3$  s with our system and  $15 \pm 3$  s with ISS ( $p > 0.05$ ).

During the naming task, our system recorded a significantly larger  $[\text{HbO}_2]$  increase ( $x \Delta[\text{HbO}_2]_{\text{L}} = 1.53 \pm 0.15 \mu\text{mol/L}$  vs.  $x \Delta[\text{HbO}_2]_{\text{R}} = 0.69 \pm 0.08 \mu\text{mol/L}$ ) ( $p = 0.02$ ) and  $[\text{Hb}]$  decrease ( $x \Delta[\text{Hb}]_{\text{L}} = -0.24 \pm 0.07 \mu\text{mol/L}$  vs.  $x \Delta[\text{Hb}]_{\text{R}} = -0.28 \pm 0.06 \mu\text{mol/L}$ ) ( $p = 0.03$ ) over the left inferior frontal area (Broca) in all four participants. A significantly larger  $[\text{HbO}_2]$  increase ( $x \Delta[\text{HbO}_2]_{\text{L}} = 2.67 \pm 0.26 \mu\text{mol/L}$  vs.  $x \Delta[\text{HbO}_2]_{\text{R}} = 1.74 \pm 0.13 \mu\text{mol/L}$ ) ( $p = 0.03$ ) and  $[\text{Hb}]$  decrease ( $x \Delta[\text{Hb}]_{\text{L}} = -0.32 \pm 0.15 \mu\text{mol/L}$  vs.  $x \Delta[\text{Hb}]_{\text{R}} = -0.28 \pm 0.09 \mu\text{mol/L}$ ) ( $p = 0.02$ ) over the left Broca area in all participants was also observed with ISS. Calculated LIs for both systems showed left hemisphere dominance for expressive language for all participants ( $\kappa = 1.0$ ,  $p < 0.0001$ ). Mean time to peak for  $\text{HbO}_2$  was  $22 \pm 3$  s (vs.  $26 \pm 2$  s for ISS) ( $p > 0.05$ ).

A strong correlation ( $0.7 < r \leq 1.0$ ) for left  $\Delta[\text{HbO}_2]$  between the two systems was obtained during the passive listening task for L1, L3 and L4. Right  $\Delta[\text{HbO}_2]$  showed a strong correlation for L1, L2 and L4 and a weak correlation ( $0.2 < r < 0.4$ ) for L3. A strong or moderate ( $0.4 < r < 0.7$ ) correlation was found for left or right  $\Delta[\text{Hb}]$  for L1, L2 and L4, while a weak correlation was found for right Hb in L3 (data not shown). For the naming task, a strong correlation for left and right  $\Delta[\text{HbO}_2]$  was obtained for all participants, except for L4 in which a weak correlation was observed for left  $\Delta[\text{HbO}_2]$ . A strong correlation for left or right  $\Delta[\text{Hb}]$  was found in three participants (L2, L3, L4) and a weak one for L1 (data not shown). Bland-Altman analysis of left and right  $\Delta[\text{HbO}_2]$  for each participant can be found in Table II. For the listening task, an overall mean difference of  $0.19 \pm 0.17 \mu\text{mol/L}$  (limits of agreement:  $-0.38$  to  $0.75 \mu\text{mol/L}$ ) was calculated for left  $\Delta[\text{HbO}_2]$  and  $0.32 \pm 0.14 \mu\text{mol/L}$  (limits of agreement:  $-0.21$  to  $0.85 \mu\text{mol/L}$ ) for its right counterpart. For the naming task, an overall mean difference of  $0.81 \pm 0.21 \mu\text{mol/L}$  (limits of agreement:  $-0.26$  to  $1.87 \mu\text{mol/L}$ ) was calculated for left  $\Delta[\text{HbO}_2]$  and  $0.69 \pm 0.16 \mu\text{mol/L}$  (limits of agreement:  $-0.30$  to  $1.68 \mu\text{mol/L}$ ) for right  $\Delta[\text{HbO}_2]$ . Figure 4 shows the hemodynamic curves and language maps during language tasks, as well as the linear regression analysis and Bland-Altman analysis for a representative participant (L3).

## Prototype Validation in Clinical Conditions

### fNIRS-EEG testing in the stroke unit

The prototype was used to investigate a 61 year-old patient admitted to the stroke unit for daily brief episodes of right upper limb shaking and leg weakness, more often

**TABLE II. Average hemodynamic changes during the language task**

Participant (sex, age, profession)		L1 (F, 26, student)	L2 (M, 22, musician)	L3 (F, 18, student)	L4 (F, 30, student)
<b>Screen distance (cm)</b>	Prot./ISS	150	142	147	147
<b>Hair description</b>	Prot./ISS	Straight, black, long	Straight, black, medium	Straight, brown, long	Straight, black, long
<b>Installation time (min)</b>	Prot./ISS	55/86	49/92	53/87	50/85
<b>Comfort scale</b>	Prot./ISS	5/2	9/2	8/4	8/4
<b>Naming task</b>					
<b>L - ΔHbO<sub>2</sub>/ΔHb (μmol)</b>	Prot.	0.75 ± 0.08	2.28 ± 0.24	1.53 ± 0.12	1.54 ± 0.15
		-0.42 ± 0.04	-0.48 ± 0.09	-0.05 ± 0.07	-0.55 ± 0.07
	ISS	1.67 ± 0.15	3.57 ± 0.35	2.40 ± 0.25	3.06 ± 0.28
		0.26 ± 0.03	0.33 ± 0.23	-1.04 ± 0.16	-0.85 ± 0.19
<b>R - ΔHbO<sub>2</sub>/ΔHb (μmol)</b>	Prot.	0.32 ± 0.05	0.91 ± 0.05	0.63 ± 0.03	0.89 ± 0.08
		-0.34 ± 0.03	-0.01 ± 0.05	-0.23 ± 0.05	-0.55 ± 0.06
	ISS	1.08 ± 0.12	2.20 ± 0.18	1.51 ± 0.13	2.17 ± 0.10
		0.05 ± 0.02	0.09 ± 0.16	-0.68 ± 0.09	-0.61 ± 0.09
<b># Words</b>	Prot./ISS	16/20	13/16	20/23	16/21
<b># Rejected trials</b>	Prot./ISS	1/3	2/3	3/2	3/3
<b>Correlation coefficient</b>	L HbO <sub>2</sub>	$r = 0.93$	$r = 0.98$ ( $p < 0.001$ )	$r = 0.99$ ( $p < 0.001$ )	$r = 0.11$ ( $p < 0.001$ )
	R HbO <sub>2</sub>	( $p < 0.001$ )	$r = 0.73$ ( $p < 0.001$ )	$r = 0.92$ ( $p < 0.001$ )	$r = 0.70$ ( $p < 0.001$ )
		$r = 0.76$			
		( $p < 0.001$ )			
<b>Differences (μmol): mean ± SD</b>	L HbO <sub>2</sub>	0.59 ± 0.13	1.05 ± 0.31	0.46 ± 0.22	1.14 ± 0.19
	R HbO <sub>2</sub>	(0.02-1.15)	(0.04-2.01)	(-0.27-1.19)	(-0.81-3.10)
		0.56 ± 0.16	0.82 ± 0.14	0.57 ± 0.22	0.80 ± 0.13
		(-0.13-1.25)	(-0.39-2.03)	(-0.15-1.30)	(-0.53-2.13)
<b>HbO<sub>2</sub> LI (dominance)</b>	Prot./ISS	0.39 (L)/0.21 (L)	0.43 (L)/0.24 (L)	0.41 (L)/0.23 (L)	0.27 (L)/0.17 (L)
<b>Passive listening task</b>					
<b>L - ΔHbO<sub>2</sub>/ΔHb (μmol)</b>	Prot.	1.28 ± 0.10	0.01 ± 0.02	0.50 ± 0.04	0.76 ± 0.07
		-0.62 ± 0.05	-0.18 ± 0.06	-0.28 ± 0.03	-0.47 ± 0.05
	ISS	0.83 ± 0.06	0.85 ± 0.06	0.46 ± 0.04	1.23 ± 0.10
		-0.25 ± 0.04	-0.21 ± 0.04	-0.33 ± 0.02	-0.45 ± 0.07
<b>R - ΔHbO<sub>2</sub>/ΔHb (μmol)</b>	Prot.	0.59 ± 0.05	0.72 ± 0.02	0.28 ± 0.03	0.37 ± 0.05
		-0.47 ± 0.04	-0.45 ± 0.04	0.04 ± 0.01	-0.32 ± 0.05
	ISS	0.55 ± 0.02	1.72 ± 0.02	0.26 ± 0.03	0.71 ± 0.04
		-0.25 ± 0.02	-0.69 ± 0.06	-0.15 ± 0.02	-0.36 ± 0.04
<b># Rejected trials</b>	Prot./ISS	4/4	5/5	4/4	5/5
<b>Correlation coefficient</b>	L HbO <sub>2</sub>	$r = 0.80$	$r = 0.17$ ( $p < 0.001$ )	$r = 0.80$ ( $p < 0.001$ )	$r = 0.88$ ( $p < 0.001$ )
	R HbO <sub>2</sub>	( $p < 0.001$ )	$r = 0.94$ ( $p < 0.001$ )	$r = 0.02$ ( $p < 0.001$ )	$r = 0.96$ ( $p < 0.001$ )
		$r = 0.66$			
		( $p < 0.001$ )			
<b>Differences (μmol): mean ± SD</b>	L HbO <sub>2</sub>	-0.22 ± 0.17	0.31 ± 0.17	0.46 ± 0.22	0.21 ± 0.14
	R HbO <sub>2</sub>	(-0.76-0.31)	(-0.23-0.85)	(-0.27-1.19)	(-0.25-0.66)
		-0.05 ± 0.04	0.60 ± 0.22	0.57 ± 0.22	0.17 ± 0.05
		(-0.54-0.43)	(-0.12-1.33)	(-0.14-1.30)	(-0.01-0.34)
<b>HbO<sub>2</sub> LI (dominance)</b>	Prot./ISS	0.37 (L)/0.20 (L)	-0.98 (R)/-0.34 (R)	0.28 (L)/0.28 (L)	0.35 (L)/0.26 (L)

M: male; F: female; HbO<sub>2</sub>: oxy-hemoglobin; Hb: deoxy-hemoglobin; L: left; R: right; Prot.: prototype; ISS: commercial fNIRS system.

while standing up for a prolonged period [Kassab et al., 2016]. Recording was started as the patient was in supine position then in a sitting position. As the patient stood up, his blood pressure decreased gradually from 134/70 to 90/54 after 10 minutes at which point he experienced tremor of the right forearm and hand as well as weakness of both legs and mild dysarthria. fNIRS showed a progressive bilateral decrease in CBV, [HbO<sub>2</sub>] and an increase in [Hb] over a one-minute period prior the beginning of the

limb-shaking (Table III and Supporting Information, Fig. 4, left). These changes rapidly normalized 15 seconds after the patient sat down and ceased to have any symptoms. Averaging the first 10s of symptom onset, hemodynamic changes were found to be most profound in bilateral right more than left dorsolateral prefrontal cortex and motor area. Similar findings were found in three other episodes of limb shaking triggered by orthostatic hypotension. In all recordings, peripheral oxygen saturation (pulse oximetry)

**TABLE III. Clinical data and average changes in HbO<sub>2</sub> concentration during the clinical recordings**

Patient	Age (sex)	Handiness (profession)	Recording duration (# blocs)	Technical issues	Diagnosis	Additional neuroimaging modalities	$\Delta$ [HbO <sub>2</sub> ] ( $\mu\text{mol/l}$ )
C1	63 (M)	R (retired)	2 × 1 h	None	LS-TIA	MRA: L occlusion of M1, R severe supraclinoid ICA stenosis ASL: decrease rCBF within the L MCA territory	$L_H^* = -1.50$ $R_H^* = -1.50$
C2	23 (F)	R (educator)	10 h	None	Bi-temporal lobe epilepsy	iSPECT: increase CBF over the middle and posterior portions of the right TL	LT = 29.75 RT = 71.09
C3	30 (F)	R (student)	24 h	Helmet not ICU-friendly	Refractory SE	iiSPECT: R posterior temporal seizure focus MEG: temporal spikes from the posterior portion of the insula and R temporal opercula	LF** = 0.49 RF** = 1.63 RT** = 0.51
C4	51 (F)	Right (retired)	8 h (N = 7)	None	Stroke, refractory epilepsy	fMRI: R language dominance	$B_L = 0.40$ $B_R = 0.85$ ( $LI_N = -0.36$ )

M: male; F: female; R: right; L: left; HbO<sub>2</sub>: oxyhemoglobin; LI: laterality index; B<sub>L</sub>: Broca left; B<sub>R</sub>: Broca right; L<sub>H</sub>: left hemisphere; R<sub>H</sub>: right hemisphere; LT: left temporal RT: right temporal; LF: left frontal; RF: right frontal; TL: temporal lobe; ICU: intensive care unit; MRA: magnetic resonance angiography; ASL: arterial spin labeling; rCBF: regional cerebral blood flow; iSPECT: ictal single position emission computed tomography; iiSPECT: interictal single positron emission computed tomography; MEG: magnetoencephalography; fMRI: functional magnetic resonance imaging; \*: one session of recording, \*\*: one burst of seizure.

was carefully monitored and remained above 95%. Simultaneous EEG monitoring showed no epileptiform abnormalities, and only brief diffuse slow (i.e. 6–7 Hz) theta activity more predominantly over the left parasagittal regions at the moment of limb shaking. Figure 5 shows blood pressure, hemoglobin concentration curves and EEG while the patient was sitting down and standing up of two episodes during the first monitoring session.

#### **fNIRS-EEG testing in the epilepsy monitoring unit**

A 23-year-old female with refractory epilepsy was admitted to the EMU to better assess her condition. During her stay, fNIRS-EEG monitoring was performed at the bedside for several hours over 2 days. A 2 minute-long subtle dyscognitive seizure was recorded starting in the right temporal region with subsequent propagation to the left temporal region based on surface EEG. Hemodynamically, fNIRS revealed an initial brief dip in HbO<sub>2</sub> at seizure onset followed by a larger increase over the middle and posterior portions of the right temporal area (Table III and Supporting Information, Fig. 4, right). A smaller HbO<sub>2</sub> increase in the anterior part of the left temporal region was also seen. A slight decrease in Hb was observed in the right temporal region but more evident over the left temporal region as the seizure evolved (approximately 40 s after the beginning of the seizure). A normalization of HbO<sub>2</sub> and Hb to approximately pre-seizure values occurred 80 s after seizure offset. Peripheral oximetry was above 98% throughout the event. No significant hemodynamic changes were seen elsewhere. SPECT images

following the injection of Tc-99m ethyl cysteinate dimer 34 seconds after seizure onset revealed increased cerebral blood flow maximal over the middle and posterior portions of the right temporal lobe as well.

#### **fNIRS-EEG testing in the intensive care unit**

A 30 year-old patient with pharmacoresistant right fronto-insular epilepsy was admitted in status epilepticus manifesting as multiple brief (~10s) asymmetrical tonic seizures. Treatment included intravenous lorazepam and phenytoin load, intubation and admission to the intensive care unit. fNIRS-EEG performed at the bedside for 24h recorded 15 brief seizures (without clinical manifestations as the patient was curarized). During these electrical seizures, fNIRS revealed fluctuations in hemoglobin concentration characterized by an increase [HbO<sub>2</sub>] in over both dorsolateral frontal (right more than left) and right lateral temporal regions (Table III and Supporting Information, Fig. 5, left). These changes were associated with a small bilateral increase in [Hb] over the dorsolateral frontal cortices. In the posterior part of the lateral temporal lobe, [Hb] increased on the right, but decrease on the left. Blood pressure and systemic oxygen saturation were stable throughout the monitoring.

#### **fNIRS-EEG testing during neuropsychological evaluation**

The prototype was used to assess language hemispheric lateralization in a 51-year-old left-handed patient as part

of the neuropsychological work-up done prior to epilepsy surgery. The patient had a past history of hemiconvulsion-hemiplegia-epilepsy (HHE) at the age of 9 months that left her with right spastic hemiparesis and refractory epilepsy. Brain MRI revealed left hippocampal sclerosis and left periventricular gliosis. Neuropsychological evaluation showed significant visuospatial memory impairment compatible with non-dominant hemisphere impairment. Bedside fNIRS performed during expressive language tasks showed right greater than left hemodynamic activations over both Broca and Wernicke's areas (LI over Broca's areas of  $-0.36$ ) (Table III and Supporting Information, Fig. 5, right). For validation, language fMRI was also obtained, confirming right hemisphere dominance. The patient subsequently underwent a left temporo-insular resection with no language complications.

## DISCUSSION

In this article, we describe a portable multichannel wireless fNIRS-EEG system (32 EEG channels; 32 NIR emitters and 32 detectors, for a total of 128 channels) that allows rapid installation and prolonged simultaneous monitoring of superficial brain electrical and hemodynamic activities at the bedside in various settings. After a first validation on an optical phantom, we successfully demonstrated the performance of our wearable high-channel diffuse optical NIRS-EEG system in both static and mobile conditions using visual and language tasks on healthy individuals.

In regard to the EEG component, expected VEPs were identified in all participants with both the prototype and the commercial EEG system, at rest or during motion, with a good level of agreement and no substantial difference in  $P_{100}$  latencies and amplitudes. Interestingly, with both systems, a significant change in  $P_{100}$  amplitude was observed in 3 participants during motion versus rest. The effect of exercise on the VEP is beyond the scope of this paper, but prior studies have noted as well that acute and regular exercise can affect the amplitude and/or latency of the different components of VEPs [Delpont et al., 1991; Ozkaya et al., 2003; Ozmerdivenli et al., 2005; Zhao et al., 2009]. In regard to the fNIRS, visual stimulation elicited in all participants the expected activation in visual areas during both non-peddalling and pedalling conditions [Kleinschmidt et al., 1996; Strangman et al., 2002; Hoge et al., 2005; Huppert et al., 2006]. Measured  $\Delta[\text{HbO}_2]$  and  $\Delta[\text{Hb}]$  was significantly different in terms of amplitude between the resting and pedalling periods at the individual level in all eight participants for  $\Delta[\text{HbO}_2]$  and in four subjects for  $\Delta[\text{Hb}]$ . The heterogeneous response in Hb between both conditions may be due to the fact that  $\text{HbO}_2$  is more prone to be influenced by changes in global hemodynamics (e.g. heart rate) than Hb [Obrig et al., 2000; Boas et al., 2004; Huppert et al., 2009; Leff et al., 2011; Kirilina et al., 2012]. In a recent publication, motor-task associated  $\Delta[\text{HbO}_2]$  were also found to be affected more than  $\Delta[\text{Hb}]$  by pedalling [Piper et al., 2014].

Naming and passive listening tasks elicited an expected increase in  $[\text{HbO}_2]$  and decrease in  $[\text{Hb}]$  respectively over the inferior frontal and posterior temporal regions predominantly in the left hemisphere [Pujol et al., 1999; Springer et al. 1999] except for one subject with an atypical response [Knecht et al. 2003] during the listening task seen with both our prototype and the commercial system. In comparison to the latter, our system performed relatively well by showing similar activation maps, no significant difference in the time to peak for  $[\text{HbO}_2]$  and  $[\text{Hb}]$  and a good kappa agreement for language dominance. Although heterogeneity in amplitude changes were noted (amplitude differences  $> 10\%$ ), there was a strong correlation between for left and right  $\Delta[\text{HbO}_2]$  and  $\Delta[\text{Hb}]$  [13/16 (81%) pairs of measurements in each language task]. It must be noted that a range of acceptable concentration variations for cognitive tasks, such as language paradigms, have not yet been reported and concentration values may significantly differ from one system to another [Colier et al. 1995; McKeating et al., 1997; Gomersall et al., 1998; Grubhofer et al., 1999; Cho et al., 2000; Yoshitani et al., 2002; Thavasoathy et al., 2002; Fellahi et al., 2013; Luengo et al., 2013; Dix et al., 2013; Gunadi et al., 2014; Ehlis et al., 2014; Hessel et al., 2014]. Such variability in concentration values between systems have been attributed to device technology (e.g. light source type, quantification method, level of sensitivity to superficial layer, sampling rate) [Wahr et al., 1996; Lloyd-Fox et al., 2010; Gunadi et al., 2014], exact location of optodes, cap differences, as well as performance of each participant.

In regard to in-hospital utilization, initial tests confirmed the feasibility of bedside recordings on patients and revealed potential clinical usefulness. In the neurovascular unit, fNIRS-EEG was able to demonstrate progressive decline in regional cerebral blood volume during postural hypotension in a patient with steno-occlusive disorder leading to transient ischemic attacks. In the epilepsy unit, fNIRS-EEG was able to visualize regional hemodynamic changes throughout a temporal lobe seizure while SPECT could only provide a single snapshot of hemodynamic changes during this seizure. In the intensive care unit, fNIRS-EEG was capable of monitoring seizures in a patient with non-convulsive status. During neuropsychological assessment, adequate language lateralization could be achieved at the bedside with the system in a left-handed patient.

## Comparison With Other "Portable" fNIRS Systems

To our knowledge, this is the only compact wireless high-channel count EEG-fNIRS device which has undergone such diverse in-lab and in-hospital testing. The growing need to study cortical function outside a tightly controlled laboratory environment without the restrictions of tabletop instruments has led in recent years to the development of wearable and/or wireless fNIRS home-made systems (Supporting Information, Tables 2 and 3).

Vaithianathan et al. (2004) were the first to design a semi-portable fNIRS system for imaging the neonatal brain. However, it was Bozkurt et al. (2005) who performed the first fNIRS recording on an infant with a portable device. Later, a series of motion resistant and multimodal (i.e. ECG, respiration, accelerometers, pulse oximetry, actigraphy) fNIRS devices was developed by the Neural System Group at Harvard [Zhang et al. 2009; Zhang et al., 2011; Zhang et al., 2014]. More recently, the mobility of the prototype version of what is now the NIRSport was evaluated by Piper et al. (2014) with eight healthy participants performing a hand-gripping task at rest and during pedalling. Moreover, for many years, simultaneous fNIRS and EEG recordings have been done by combining two independent and non-portable systems [Leamy et al., 2011; Kaiser et al., 2014; Khan et al., 2013; Putze et al., 2014; Khan and Hong 2017]. Apart from our group (Lareau et al., 2011a,b; Sawan et al., 2012, 2013), only two other groups have designed a true hybrid fNIRS-EEG system albeit testing was limited to only a few healthy participants and with fewer channels (Safaie et al., 2013; von Lümann et al., 2015).

Parallel progress on homemade fNIRS systems, improvements have been made on commercially available wearable fNIRS systems with now the possibility to measure brain activity on two or more people simultaneously (e.g. fNIR100AW), outdoors or during physical activity (e.g. PortaLite, LIGHTNIRS, NIRSport), with very high spatial sampling (e.g. WOT-100), and/or with cytochrome c oxidase values (e.g. B&W Tek, Avantes, Ocean Optics) [Supporting Information, Table 2]. In comparison to these devices, our system can support a higher number of NIRS optodes that allow sampling of a large portion of the superficial cortex. Furthermore, while several of these companies have made their system compatible with other instruments (ex. EEG), these additional physiological signals come with longer setup time, decrease wearability/mobility and require complex synchronization.

While not the focus of this work, an important feature of our system was the design of an fNIRS-EEG cap. The challenge here was threefold, 1) to provide a stable optical contact with the scalp, 2) to ensure comfort during long-term monitoring and 3) to allow simultaneous fNIRS-EEG signal acquisition. After testing several prototypes using different stretchable material and different form of sockets and optodes housing, we were able to build an easy to use, motion-resistant and comfortable cap [Tables (I–III) and Supporting Information, Table 1]. The large socket opening and the space between holes allow pushing hair aside to improve signal quality (Idelson et al., 2015).

### Limitations

Some limitations in our study need to be pointed out. First, the portable system was tested on a small number of hospitalized patients and larger clinical studies are obviously required. Second, although a small number of short distance optodes were planned in our original design to

assess the contribution of extracerebral superficial layers to the signal, they were not yet available in our first-generation caps. Future recordings will include this component. Third, our prototype only allowed each source to be coupled to a maximum of four detectors. Albeit this allowed for quasi-full head coverage, raising the number of detected per source could provide denser coverage. Fourth, the current optode design do not allow for occipital recording while the participant is in supine position.

### Future Perspectives

Case studies provided in this paper represent only a few potential applications of a portable multichannel fNIRS-EEG system for long-term monitoring in a hospital environment. Other areas that may benefit from such neuroimaging technology include the operating room (ex. cardiac and vascular surgeries) [Maldonado et al. 2014; Kato et al. 2015], the neurosurgical critical care unit (ex. monitoring of seizures or vasospasm) [Yokose et al., 2010; Keller et al., 2015; Seule et al., 2015; Tanaka et al., 2015] and rehabilitation centers (ex. study of brain plasticity after injury) [Strangman et al., 2006; Arenth et al., 2007; Mihara et al., 2007, 2010; Yoshino et al., 2013; Khan et al., 2013]. These clinical avenues will obviously need to be explored in larger series.

In terms of technical development, incorporating other improvements made by other groups can be explored such as probe miniaturization [Kanayama and Niwayama, 2014], computer-free systems [Si et al., 2015], broadband devices [Chitnis et al., 2016], wireless fNIRS probes [Abtahi et al., 2016], portable diffuse optical topography [Atsumori et al., 2007; Kiguchi et al. 2012; Flexman et al., 2012], and integration of smartphone technology [Yurts- ever et al., 2003; Bunce et al., 2006; Sharieh et al., 2012; Watanabe et al., 2016a].

### CONCLUSIONS

To answer the need of portability to monitor electrical and hemodynamic brain activities in clinical settings, we developed a novel high channel (128 NIRS and 32 EEG) count and lightweight instrument that can display real-time changes in HbO<sub>2</sub>, Hb, HbT and EEG on a portable personal computer through a wireless wearable module. Using visual and language tasks, we established that haemodynamic activations can be retrieved. In-hospital testing on patients with various neurological conditions demonstrated the portability of the device and the potential to provide useful clinical information.

### ACKNOWLEDGEMENTS

The authors declare no conflict of interest and have nothing to disclose.

## REFERENCES

- Aasted CM, Yücel MA, Cooper RJ, Dubb J, Tsuzuki D, Becerra L, Petkov MP, Borsook D, Dan I, Boas DA (2015): Anatomical guidance for functional near-infrared spectroscopy: Atlas-Viewer tutorial. *Neurophotonics* 2:020801.
- Abtahi M, Cay G, Saikia MJ, Mankodiya K (2016): Designing and testing a wearable, wireless fNIRS patch. *Conf Proc IEEE Eng Med Biol Soc* 2016: Aug; 2016:6298–6301.
- Arenth PM, Ricker JH, Schultheis MT (2007): Applications of functional near-infrared spectroscopy (fNIRS) to neurorehabilitation of cognitive disabilities. *Clin Neuropsychol* 21:38–57.
- Atsumori H, Kiguchi M, Obata A, Sato H, Katura T, Utsugi K, Funane T, Maki A (2007): Development of a multi-channel, portable optical topography system. *Conf Proc IEEE Eng Med Biol Soc* 2007:3362–3364.
- Bland JM, Altman DG (1996): Measurement error. *BMJ Br Med J* 312:1654.
- Bland JM, Altman DG (1986): Statistical methods for assessing agreement between two methods of clinical measurement. *Lancet* Feb 81:307–310.
- Boas DA, Dale AM, Franceschini MA (2004): Diffuse optical imaging of brain activation: Approaches to optimizing image sensitivity, resolution, and accuracy. *NeuroImage* 23: S275–S288. Review.
- Boas DA, Elwell CE, Ferrari M, Taga G (2014): Twenty years of functional near-infrared spectroscopy: Introduction for the special issue. *NeuroImage* 85:1–5. Jan 15
- Bozkurt A, Rosen A, Rosen H, Onaral B (2005): A portable near infrared spectroscopy system for bedside monitoring of newborn brain. *Biomed Eng Online* Apr 29; 4:29.
- Bunce SC, Izzetoglu M, Izzetoglu K, Onaral B, Pourrezaei K (2006): Functional near-infrared spectroscopy. *IEEE Eng Med Biol Mag* Jul-Aug 25:54–62.
- Cerbo RM, Cabano R, Di Comite A, Longo S, Maragliano R, Stronati M (2012): Cerebral and somatic rSO<sub>2</sub> in sick preterm infants. *J Matern Fetal Neonatal Med* 25:97–100. Oct
- Chitnis D, Airantzis D, Highton D, Williams R, Phan P, Giagka V, Powell S, Cooper RJ, Tachtsidis I, Smith M, Elwell CE, Hebden JC, Everdell N (2016): Towards a wearable near infrared spectroscopic probe for monitoring concentrations of multiple chromophores in biological tissue in vivo. *Rev Sci Instrum* Jun87: 065112.
- Cho H, Nemoto EM, Sanders M, Fernandez K, Yonas H (2000): Comparison of two commercially available near-infrared spectroscopy instruments for cerebral oximetry. *Technical note. J Neurosurg* 93:351–354.
- Colier WN, van Haaren NJ, Oeseburg B (1995): A comparative study of two near infrared spectrophotometers for the assessment of cerebral haemodynamics. *Acta Anaesthesiol Scand* 39: 101–105. SupplPubMed PMID: 8599259.
- Cooper CE, Elwell CE, Meek JH, Matcher SJ, Wyatt JS, Cope M, Delpy DT (1996): The non-invasive measurement of absolute cerebral deoxyhemoglobin concentration and mean optical path length in the neonatal brain by second derivative near infrared spectroscopy. *Pediatr Res* 39:32–38.
- Cox DR, Wermuth N (1996): *Multivariate Dependencies: Models, Analysis and Interpretation*. London: Chapman and Hall/CRC Reference. p 272.
- Delpont E, Dolisi C, Suisse G, Bodino G, Gastaud M (1991): Visual evoked potentials: Differences related to physical activity. *Int J Sports Med* 12:293–298.
- Delpy DT, Cope M, v, der Zee P, Arridge S, Wray S, Wyatt J (1988): Estimation of optical pathlength through tissue from direct time of flight measurement. *PhysMed Biol* Dec 33:1433–1442.
- Denault A, Deschamps A, Murkin JM (2007): A proposed algorithm for the intraoperative use of cerebral near-infrared spectroscopy. *Semin Cardiothorac Vasc Anesth* 11:274–281.
- Dice LR (1945): Measures of the amount of ecologic association between species. *Ecology* 26:297–302.
- Dix LM, van Bel F, Baerts W, Lemmers PM (2013): Comparing near-infrared spectroscopy devices and their sensors for monitoring regional cerebral oxygen saturation in the neonate. *Pediatr Res* 74:557–563.
- Duncan A, Meek JH, Clemence M, Elwell CE, Tyszczyk L, Cope M, Delpy DT (1995): Optical pathlength measurements on adult head, calf and forearm and the head of the newborn infant using phase resolved optical spectroscopy. *Phys Med Biol* 40:295–304.
- Edmonds HL, Jr, Ganzel BL, Austin EH 3rd (2004): Cerebral oximetry for cardiac and vascular surgery. *Semin Cardiothorac Vasc Anesth* 8:147–166.
- Ehlis AC, Schneider S, Dresler T, Fallgatter AJ (2014): Application of functional near-infrared spectroscopy in psychiatry. *NeuroImage* 85 Pt 1:478–488. Jan 15
- Fellahi JL, Butin G, Fischer MO, Zamparini G, Gérard JL, Hanouz JL (2013): Dynamic evaluation of near-infrared peripheral oximetry in healthy volunteers: A comparison between INVOS and EQUANOX. *J Crit Care* 28:881.e1–886.
- Ferrari M, Giannini I, Sideri G, Zanette E (1985): Continuous non-invasive monitoring of human brain by near infrared spectroscopy. *Adv Exp Med Biol* 191:873–882.
- Ferrari M, Quaresima V (2012): A brief review on the history of human functional near-infrared spectroscopy (fNIRS) development and fields of application. *NeuroImage* 63:921–935. Nov 1
- Flexman ML, Kim HK, Stoll R, Khalil MA, Fong CJ, Hielscher AH (2012): A wireless handheld probe with spectrally constrained evolution strategies for diffuse optical imaging of tissue. *Rev Sci Instrum* 83:033108.
- Gallagher A, Thériault M, Maclin E, Low K, Gratton G, Fabiani M, Gagnon L, Valois K, Rouleau I, Sauerwein HC, Carmant L, Nguyen DK, Lortie A, Lepore F, Béland R, Lassonde M (2007): Near-infrared spectroscopy as an alternative to the Wada test for language mapping in children, adults and special populations. *Epileptic Disord* Sep 9:241–255.
- Gomersall CD, Leung PL, Gin T, Joynt GM, Young RJ, Poon WS, Oh TE (1998): A comparison of the Hamamatsu NIRO 500 and the INVOS 3100 near-infrared spectrophotometers. *Anaesth Intensive Care* Oct 26:548–557.
- Grubhofer G, Tonninger W, Keznickl P, Skyllouriotis P, Ehrlich M, Hiesmayr M, Lassnigg A (1999): A comparison of the monitors INVOS 3100 and NIRO 500 in detecting changes in cerebral oxygenation. *Acta Anaesthesiol Scand* 43:470–475.
- Gunadi S, Leung TS, Elwell CE, Tachtsidis I (2014): Spatial sensitivity and penetration depth of three cerebral oxygenation monitors. *Biomed Opt Express* Aug 5:2896–2912. 1
- Hessel TW, Hyttel-Sorensen S, Greisen G (2014): Cerebral oxygenation after birth – a comparison of INVOS® and FORE-SIGHT™ near-infrared spectroscopy oximeters. *Acta Paediatr* 103:488–493.
- Hoge RD, Franceschini MA, Covolan RJ, Huppert T, Mandeville JB, Boas DA (2005): Simultaneous recording of task-induced changes in blood oxygenation, volume, and flow using diffuse optical imaging and arterial spin-labeling MRI. *NeuroImage* 25:701–707. Apr 15

- Huppert TJ, Hoge RD, Diamond SG, Franceschini MA, Boas DA (2006): A temporal comparison of BOLD, ASL, and NIRS hemodynamic responses to motor stimuli in adult humans. *NeuroImage* 29:368–382. Jan 15
- Huppert TJ, Diamond SG, Franceschini MA, Boas DA (2009): HomER: A review of time-series analysis methods for near-infrared spectroscopy of the brain. *Appl Opt* 48:D280–D298.
- Idelson CR, Vogt WC, King-Casas B, LaConte SM, Rylander CG (2015): Effect of mechanical optical clearing on near-infrared spectroscopy. *Lasers Surg Med* 47:495–502.
- Jöbsis FF, Keizer JH, LaManna JC, Rosenthal M (1977): Reflectance spectrophotometry of cytochrome aa3 in vivo. *J Appl Physiol Respir Environ Exerc Physiol* 43:858–872.
- Kaiser V, Bauernfeind G, Kreiling A, Kaufmann T, Kübler A, Neuper C, Müller-Putz GR (2014): Cortical effects of user training in a motor imagery based brain-computer interface measured by fNIRS and EEG. *NeuroImage* 85:432–444.
- Kanayama N, Niwayama M (2014): Examiner’s finger-mounted fetal tissue oximetry. *J Biomed Opt* 19:067008.
- Kassab A, Tremblay J, Poppe AY, Létourneau-Guillon L, Gallagher A, Nguyen DK (2016): Cerebral hemodynamic changes during limb-shaking TIA: A near-infrared spectroscopy study. *Neurology* Mar 2286:1166–1168.
- Kato S, Yoshitani K, Ohnishi Y (2015): Cerebral blood flow measurement by near-infrared spectroscopy during carotid endarterectomy. *J Neurosurg Anesthesiol* Aug 28.
- Keller E, Froehlich J, Baumann D, Böcklin C, Sikorski C, Oberle M, Muser M (2015): Detection of delayed cerebral ischemia (DCI) in subarachnoid haemorrhage applying near-infrared spectroscopy: Elimination of the extracerebral signal by transcutaneous and intraparenchymatous measurements in parallel. *Acta Neurochir Suppl* 120:243–247.
- Khan B, Hodics T, Hervey N, Kondraske G, Stowe AM, Alexandrakis G (2013): Functional near-infrared spectroscopy maps cortical plasticity underlying altered motor performance induced by transcranial direct current stimulation. *J Biomed Opt* 18:116003.
- Khan MJ, Hong KS (2017): Hybrid EEG-fNIRS-based eight-command decoding for BCI: Application to quadcopter control. *Front Neurobot* Feb 17; 11:6.
- Kohri S, Hoshi Y, Tamura M, Kato C, Kuge Y, Tamaki N (2002): Quantitative evaluation of the relative contribution ratio of cerebral tissue to near-infrared signals in the adult human head: A preliminary study. *Physiol Meas* 23:301–312.
- Kiguchi M, Atsumori H, Fukasaku I, Kumagai Y, Funane T, Maki A, Kasai Y, Ninomiya A (2012): Note: Wearable near-infrared spectroscopy imager for haired region. *Rev Sci Instrum* 83: 056101.
- Kirilina E, Jelzow A, Heine A, Niessing M, Wabnitz H, Brühl R, Ittermann B, Jacobs AM, Tachtsidis I (2012): The physiological origin of task-evoked systemic artefacts in functional near infrared spectroscopy. *NeuroImage* 61:70–81. May 15
- Kleinschmidt A, Obrig H, Requardt M, Merboldt KD, Dirnagl U, Villringer A, Frahm J (1996): Simultaneous recording of cerebral blood oxygenation changes during human brain activation by magnetic resonance imaging and near-infrared spectroscopy. *J Cereb Blood Flow Metab* 16:817–826. SepPubMed PMID: 8784226.
- Knecht S, Jansen A, Frank A, van Randenborgh J, Sommer J, Kanowski M, Heinze HJ (2003): How atypical is atypical language dominance?. *NeuroImage* 18:917–927.
- Kocsis L, Herman P, Eke A (2006): The modified Beer-Lambert law revisited. *Phys Med Biol* 51:N91–N98. Mar 7
- Kopton IM, Kenning P (2014): Near-infrared spectroscopy (NIRS) as a new tool for neuroeconomic research. *Front Hum Neurosci* 8:549.
- Lareau E, Lesage F, Pouliot P, Nguyen D, Le Lan J, Sawan M (2011): Multichannel wearable system dedicated for simultaneous electroencephalography and near-infrared spectroscopy real-time data acquisitions. *J Biomed Opt* 16:096014.
- Lareau E, Simard G, Lesage F, Nguyen D and Sawan M (2011): “Near infrared spectrometer combined with multichannel EEG for functional brain imaging,” 5th International Symposium on Medical Information and Communication Technology, Montreux, 2011, pp. 122–126.
- Leamy, Darren J. and Collins, Ronan and Ward, Tomas E (2011): Combining fNIRS and EEG to improve motor cortex activity classification during an imagined movement-based task. In: FAC’11 Proceedings of the 6th international conference on Foundations of augmented cognition: directing the future of adaptive systems.
- Leff DR, Orihuela-Espina F, Elwell CE, Athanasiou T, Delpy DT, Darzi AW, Yang GZ (2011): Assessment of the cerebral cortex during motor task behaviours in adults: A systematic review of functional near infrared spectroscopy (fNIRS) studies. *NeuroImage* 54:2922–2936. Feb 14
- Lloyd-Fox S, Blasi A, Elwell CE (2010): Illuminating the developing brain: The past, present and future of functional near infrared spectroscopy. *Neurosci Biobehav Rev* 34:269.
- Luengo C, Resche-Rigon M, Damoiseil C, Kerever S, Creteur J, Payen D (2013): Comparison of two different generations of “NIRS” devices and transducers in healthy volunteers and ICU patients. *J Clin Monit Comput* 27:71–79.284.
- Madsen PL, Secher NH (1999): Near-infrared oximetry of the brain. *Prog Neurobiol* 58:541–560.
- Maldonado Y, Singh S, Taylor MA (2014): Cerebral near-infrared spectroscopy in perioperative management of left ventricular assist device and extracorporeal membrane oxygenation patients. *Curr Opin Anaesthesiol* 27:81–88.
- McKeating EG, Monjardino JR, Signorini DF, Souter MJ, Andrews PJ (1997): A comparison of the InVivo 3100 and the Critikon 2020 near-infrared spectrophotometers as monitors of cerebral oxygenation. *Anaesthesia* 52:136–140.
- Mihara M, Miyai I, Hatakenaka M, Kubota K, Sakoda S (2007): Sustained prefrontal activation during ataxic gait: A compensatory mechanism for ataxic stroke?. *NeuroImage* 37:1338–1345. Oct 1
- Mihara M, Yagura H, Hatakenaka M, Hattori N, Miyai I (2010): Clinical application of functional near-infrared spectroscopy in rehabilitation medicine. *Brain Nerve* Feb62:125–132.
- Mihara M, Miyai I (2016): Review of functional near-infrared spectroscopy in neurorehabilitation. *Neurophotonics* Jul3:031414.
- Murkin JM, Arango M (2009): Near-infrared spectroscopy as an index of brain and tissue oxygenation. *Br J Anaesth* 103:i3–13. Dec
- Naseer N, Hong K-S (2015): fNIRS-based brain-computer interfaces: A review. *Front Hum Neurosci* 9:3.
- Obrig H, Neufang M, Wenzel R, Kohl M, Steinbrink J, Einhäupl K, Villringer A (2000): Spontaneous low frequency oscillations of cerebral hemodynamics and metabolism in human adults. *NeuroImage* 12:623–639.
- Obrig H (2014): NIRS in clinical neurology - a ‘promising’ tool?. *NeuroImage* 85 Pt 1:535–546. Jan 15
- Oldfield RC (1971): The assessment and analysis of handedness: The Edinburgh inventory. *Neuropsychologia* Mar 9: 97–113.
- Ozkaya YG, Agar A, Hacıoglu G (2003): Training induced alterations of visual evoked potentials are not related to body temperature. *Int J Sports Med* 24:359–362.



- Ozmerdivenli R, Bulut S, Bayar H, Karacabey K, Ciloglu F, Peker I, Tan U (2005): Effects of exercise on visual evoked potentials. *Int J Neurosci* 115:1043–1050.
- Piper SK, Krueger A, Koch SP, Mehnert J, Habermehl C, Steinbrink J, Obrig H, Schmitz CH (2014): A wearable multi-channel fNIRS system for brain imaging in freely moving subjects. *NeuroImage* Jan 1585: 64–71.
- Psychology Software Tools, Inc. [E-Prime 2.0]. 2012. Retrieved from <http://www.pstnet.com>.
- Pujol J, Deus J, Losilla JM, Capdevila A (1999): Cerebral lateralization of language in normal left-handed people studied by functional MRI. *Neurology* 52:1038–1043. Mar 23
- Putze F, Hesslinger S, Tse CY, Huang Y, Herff C, Guan C, Schultz T (2014): Hybrid fNIRS-EEG based classification of auditory and visual perception processes. *Front Neurosci* 8:373. Nov 18;
- Safaie J, Grebe R, Abrishami Moghaddam H, Wallois F (2013): Toward a fully integrated wireless wearable EEG-NIRS bimodal acquisition system. *J Neural Eng* 10:056001.
- Sawan M, Salam MT, Gelinis S, Le Lan J, Lesage F, Nguyen DK (2012): Combined NIRS-EEG remote recordings for epilepsy and stroke real-time monitoring, 2012 IEEE International Symposium on Circuits and Systems, Seoul, Korea (South), pp. 13–16.
- Sawan M, Salam MT, L, Lan J, Kassab A, Gelinis S, Vannasing P, Lesage F, Lassonde M, Nguyen DK (2013): Wireless recording systems: From noninvasive EEG-NIRS to invasive EEG devices. *IEEE Trans Biomed Circuits Syst* Apr7:186–195.
- Scholkmann F, Kleiser S, Metz AJ, Zimmermann R, Mata Pavia J, Wolf U, Wolf M (2014): A review on continuous wave functional near-infrared spectroscopy and imaging instrumentation and methodology. *NeuroImage* 85:6–27. Jan 15
- Seghier ML (2008): Laterality index in functional MRI: Methodological issues. *Magn Reson Imaging* 26:594–601.
- Seule M, Keller E, Unterberg A, Sakowitz O (2015): The hemodynamic response of spreading depolarization observed by near infrared spectroscopy after aneurysmal subarachnoid hemorrhage. *Neurocrit Care* 23:108–112.
- Si J, Zhao R, Zhang Y, Zuo N, Zhang X, Jiang T (2015): A portable fNIRS system with eight channels. *Proc. SPIE 9305, Optical Techniques in Neurosurgery, Neurophotonics, and Optogenetics II*, 93051B (March 10, 2015).
- Springer JA, Binder JR, Hammcke TA, Swanson SJ, Frost JA, Bellgowan PS, Brewer CC, Perry HM, Morris GL, Mueller WM (1999): Language dominance in neurologically normal and epilepsy subjects: A functional MRI study. *Brain* 122:2033–2046. Nov
- Strangman G, Boas DA, Sutton JP (2002): Non-invasive neuroimaging using near-infrared light. *Biol Psychiatry* 52:679–693. Oct 1 Review.
- Strangman G, Goldstein R, Rauch SL, Stein J (2006): Near-infrared spectroscopy and imaging for investigating stroke rehabilitation: Test-retest reliability and review of the literature. *Arch Phys Med Rehabil* 87:S12–S19.
- Tanaka Y, Ebihara A, Ikota M, Yamaguro T, Kamochi H, Kusaka G, Ishikawa M, Konno T, Mashiko T, Watanabe E (2015): Early diagnosis of cerebral ischemia in cerebral vasospasm by oxygen-pulse near-infrared optical topography. *Acta Neurochir Suppl* 120:269–274.
- Thavasoathy M, Broadhead M, Elwell C, Peters M, Smith M (2002): A comparison of cerebral oxygenation as measured by the NIRO 300 and the INVOS 5100 Near-Infrared Spectrophotometers. *Anaesthesia* 57:999–1006.
- Torricelli A, Contini D, Pifferi A, Caffini M, Re R, Zucchelli L, Spinelli L (2014): Time domain functional NIRS imaging for human brain mapping. *NeuroImage* 85:28–50. Jan 15
- Vaithianathan T, Tullis IDC, Everdell N, Leung T, Gibson A, Meek J, Delpy DT (2004): Design of a portable near-infrared system for topographic imaging of the brain in babies. *Rev Sci Instrum* 75:3276–3283.
- Villringer A, Chance B (1994): Non-invasive optical spectroscopy and imaging of human brain function. *Trends Neurosci* Oct20: 435–442.
- von Lüthmann A, Herff C, Heger D, Schultz T (2015): Toward a wireless open source instrument: Functional near-infrared spectroscopy in mobile neuroergonomics and BCI applications. *Front Hum Neurosci* 9:617.
- Wahr JA, Tremper KK, Samra S, Delpy DT (1996): Near-infrared spectroscopy: Theory and applications. *J Cardiothorac Vasc Anesth* 10:406–418.
- Watanabe T, Sekine R, Mizuno T, Miwa M (2016): Development of portable, wireless and smartphone controllable near-infrared spectroscopy system. *Adv Exp Med Biol* 923:385–392.
- Wolf M, Ferrari M, Quaresima V (2007): Progress of near-infrared spectroscopy and topography for brain and muscle clinical applications. *J Biomed Opt* Nov-Dec12:062104.
- Yoshino K, Oka N, Yamamoto K, Takahashi H, Kato T (2013): Functional brain imaging using near-infrared spectroscopy during actual driving on an expressway. *Front Hum Neurosci* 7:882.
- Yokose N, Sakatani K, Murata Y, Awano T, Igarashi T, Nakamura S, Hoshino T, Katayama Y, (2): (2010): Bedside monitoring of cerebral blood oxygenation and hemodynamics after aneurysmal subarachnoid hemorrhage by quantitative time-resolved near-infrared spectroscopy. *World Neurosurg* 73:508–513.
- Yoshitani K, Kawaguchi M, Tatsumi K, Kitaguchi K, Furuya H (2002): A comparison of the INVOS 4100 and the NIRO 300 near-infrared spectrophotometers. *Anesth Analg* 94: 586–590.
- Zijdenbos AP, Dawant BM, Margolin RA, Palmer AC (1994): Morphometric analysis of white-matter lesions in MR-images — method and validation. *IEEE Trans Med Imaging* 13: 716–724.
- Zhang Y, Sun JW, Wei G, Scopesi F, Serra G, Rolfe P (2009): Design of a Portable Near Infra-Red Spectroscopy System for Tissue Oxygenation Measurement. 3rd International Conference on Bioinformatics and Biomedical Engineering, Beijing, 2009, pp. 1–4.
- Zhang Q, Yan X, Strangman GE (2011): Development of motion resistant instrumentation for ambulatory near-infrared spectroscopy. *J Biomed Opt* 16:087008.
- Zhang Q, Ivkovic V, Hu G, Strangman GE (2014): Twenty-four-hour ambulatory recording of cerebral hemodynamics, systemic hemodynamics, electrocardiography, and actigraphy during people’s daily activities. *J Biomed Opt* 19:47003.
- Zhao J, Pang S, Che G (2009): Specificity and sensitivity of visual evoked potentials P100 latency to different events exercise. *Health* 1:47–50.